Long-Distance Crosswell EM Logging of Copper Ore Using Borehole-Surface Current Injection in Slim Holes

Jingxin Dang [ORCID], *Student Member, IEEE*, Qing Zhao [ORCID], Cheng Guo, Jiadai Li, Lei Zhang, Tianzhi Tang, Bo Dang [ORCID], *Member, IEEE*, Ling Yang, *Student Member, IEEE*, and Changzan Liu [ORCID], *Student Member, IEEE*

Abstract—Crosswell electromagnetic (EM) methods are widely used in subsurface geophysical prospecting because they can achieve more effective long-distance detection than single-well methods. However, a large-diameter borehole is required to increase the magnetic moment of the magnetic dipole source. For the long-distance detection of copper ores, which is usually performed in slim holes, we present a borehole-surface current-injection-based crosswell EM logging method. Considering the cost of deploying casing, we inject a low-frequency ac directly into the ground, and converging current is formed around low-resistance anomalies in the formation. Then, the distribution of the anomalies can be inferred by detecting the low-frequency alternating magnetic field of the converging current in the receiver well. Moreover, to further improve the detection performance, we design a placement scheme for the grounding electrode for multianomaly crosswell detection based on the Gauss–Newton inversion algorithm, where the EM responses for different grounding electrode locations are analyzed. Field experiments are conducted using two slim open holes spaced approximately 1000 m apart for the detection of two copper ores. Through the processing and interpretation of measured EM signals, the conductivity imaging results of the crosswell EM method indicate that the measured distribution of anomalies is consistent with prior knowledge obtained from numerous single-well loggings, demonstrating the feasibility of the proposed application for long-distance crosswell EM logging in slim open holes.

Index Terms—Copper ore, crosswell electromagnetic (EM) method, current injection, long distance, slim open hole.

I. INTRODUCTION

IN RECENT years, underground resources have been increasingly exploited, and precise knowledge of the properties of subterranean formation is necessary for further resource

Jingxin Dang, Qing Zhao, Cheng Guo, Jiadai Li, and Lei Zhang are with the School of Resources and Environment, University of Electronic Science and Technology of China, Chengdu 610056, China (e-mail: 15029276190@163.com; zhaoq@uestc.edu.cn; guocheng@uestc.edu.cn; ljd@uestc.edu.cn; 827031540@qq.com).

Tianzhi Tang is with the China National Logging Corporation, China National Petroleum Corporation, Beijing 100007, China (e-mail: tangtz@cnpc.com.cn).

Bo Dang, Ling Yang, and Changzan Liu are with the Key Laboratory of Education Ministry for Photoelectric Logging and Detecting of Oil and Gas, Xi'an Shiyou University, Xi'an 710312, China (e-mail: bodang521@126.com; lingyang2915@163.com; liuchangzan@mail.nwpu.edu.cn).

Digital Object Identifier 10.1109/JSTARS.2022.3189817

exploration and development [1]. The classical surface-based methods (such as controlled-source EM and magnetotelluric methods) are effective in obtaining stratigraphic information, however, due to the fact that its detection devices are deployed on the surface far from the targets deep in the stratum (such as deep ore bodies), it is challenging to achieve high accuracy detection in large depth environments [2]–[4]. Earlier subsurface resource exploration was often achieved by single-well logging [5]. However, for copper ore detection, numerous single-well loggings are required to obtain the distribution of the target, resulting in enormous cost. The crosswell electromagnetic (EM) method is an important geophysical exploration method that extends the research scope of traditional single-well logging and can obtain the formation conductivity distribution over a large area between wells [6]. This method is widely used for reservoir characterization, flood monitoring, oil and gas identification, and mineral exploration [7]–[10].

A crosswell EM system typically uses a magnetic dipole source as a transmitter deployed in the transmitter well to broadcast a time-varying magnetic field. A high-sensitivity magnetic probe that detects the EM field is deployed in the receiver well at a certain distance from the transmitting well [11]–[14]. Since a high-frequency EM wave attenuates too rapidly in the formation, low frequencies between 5 Hz and tens of kHz are generally used for crosswell detection [15]–[19]. EMI Company developed the XBH2000 system using an iterative Born inversion technique to achieve resistivity inversion of the formation between two wells spaced up to 500 m apart [20], [21]. Through continuous improvement and refinement, the DeepLook-EM logging system developed by Schlumberger uses an array of magnetic probes to detect signals, which not only reduces the outside diameter of the receiver, but also increases the detection sensitivity to 10^{-6} nT, thus enabling crosswell EM logging between wells spaced up to 1000 m apart [22]. However, long-distance crosswell logging requires the source to have a large magnetic moment, which means that the excitation current, number of turns, and cross-sectional area of the transmitting coil need to be as large as possible. As a result, the transmitter must be very large [23]. All of the magnetic transmitters used in the above-mentioned studies have an outside diameter of 8 cm or more, and the required borehole diameter is at least 11.5 cm, which makes it difficult to achieve long-distance logging between small-diameter (<50 mm) wells.

In contrast to devices using a magnetic source, devices using an electrical source can use high power to expand the radiation range and are thus more suitable for deep exploration [24]–[26]. In addition, some researchers have investigated the fields generated by electrical and magnetic sources, and demonstrated that an electrical source can excite EM fields in both TE and TM polarization modes in the subsurface (where TE mode and TM mode are dependent upon the transverse electric waves and the transverse magnetic waves, respectively) [27], [28]. Considering the complexity of the downhole environment and the safety of operation, crosswell EM detection methods based on electrical sources generally employ small-size electric dipole sources instead of long-wire sources [29]. Yu and Edwards [30] simulated an electric dipole–dipole system with a whole-space response between wells and demonstrated that the method is capable of crosswell detection with a well spacing of 100 m [31]. To further increase the radial detection distance, some researchers utilized the high electrical conductivity of metal casing and regarded a long metal-cased borehole as a vertical line source, which could significantly enhance the transmission power and enable crosswell detection over several hundreds or even thousands of meters [32]–[34]. However, considering the cost of deploying casing, open holes are typically used for metal ore exploration. After obtaining stratigraphic information, the test wells are filled in time to avoid collapse. Therefore, when using open holes, we cannot achieve long-distance detection by utilizing metal casing.

In the case of using an open hole as the transmitter well, Kuckes *et al.* [35] proposed an extended lateral range electrical conductivity logging technique using a current injection source to achieve relief well positioning, in which the electrical device and detection module are deployed in the relief well (open hole). A low-frequency ac is injected directly into the formation, and the blowout well casing is used to converge the current to generate a low-frequency magnetic field. The relative position information from the relief well to the blowout well can be estimated by analyzing the collected magnetic field signals. Based on this method, He *et al.* [36] proposed a borehole-surface time-frequency EM technique that uses a downhole current injection electrode and a surface grounding electrode to obtain EM signals to analyze the reservoir range and boundary of the oil well. In addition, Hu *et al.* [37] described a design of electrical impedance tomography (EIT) using electrodes and magnetic devices for the reconstruction of high-contrast proppant in hydraulic fractures, similarly implemented by the joint use of surface and downhole instruments. The theories and tools for the methods as EIT or current injection have already been developed in geophysical fields such as relief well drilling and reservoir imaging [38], but the application of them for long-distance crosswell detection of copper ores in slim open holes has not yet been realized. Therefore, this article focuses on realizing a new application of such typical methods.

As discussed earlier, the currently available long-distance detection systems are hardly effective in the environment with slim open holes and large well spacing. Inspired by the current injection method, we propose a long-distance crosswell EM logging method using borehole-surface current injection in this
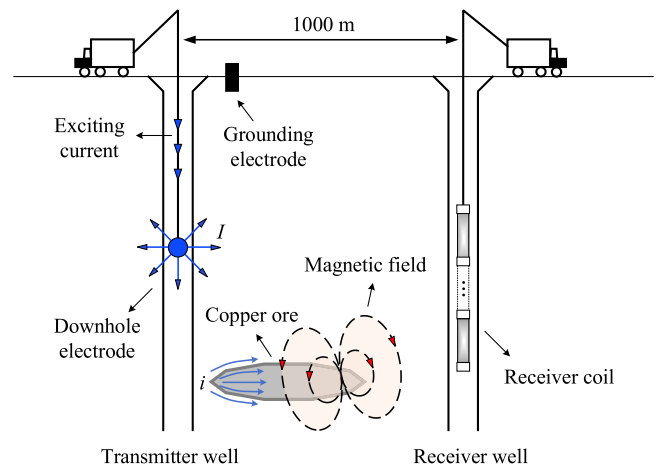

Fig. 1. Crosswell system model using the borehole-surface current injection method.

article. Unlike the traditional current injection or EIT method mentioned earlier, the current-injection-based method presented in this article requires receivers to be placed in the well rather than on the surface. Specifically, we use a downhole electrode as the transmitter to inject a large low-frequency ac into the ground, and place a grounding electrode on the surface to guide the direction of current flow. Considering the high electrical conductivity of metal anomalies in the formation, we use these low-resistance bodies to converge currents and generate alternating magnetic fields, thus enhancing the strength of the EM signals in the receiver well for long-distance detection. To verify the feasibility of the presented new application, we first establish the system models, and perform the simulations of the whole-space response. Furthermore, a grounding electrode placement scheme is designed to improve the detection performance. Based on this, a series of large-scale field experiments are conducted. To ensure the practicability of the experiment, we make some adjustments and improvements to the structure of instruments according to the actual environment, such as the size of the probe, the number of turns and the connection modes between multiple probes, etc. The processing results of the measured data indicate that the stratigraphic information obtained by the proposed method is in good agreement with prior logging information.

The remainder of this article is organized as follows. In Section II, a current-injection-based crosswell system model is constructed, and the theoretical analysis of the cylindrical model is presented. In Section III, an irregular multianomaly crosswell system model is built, and the whole-space response is simulated. In Section IV, the design of the grounding electrode placement is presented. In Section V, the field test is described, and the processing results of the measured data are presented. Finally, Section VI concludes this article.

II. CROSSWELL SYSTEM MODEL USING BOREHOLE-SURFACE CURRENT INJECTION

As illustrated in Fig. 1, the transmitter system is composed of a downhole electrode and a grounding electrode, and the receiver system is an array consisting of multiple high-sensitivity receiver

coils. The distance between the transmitter and receiver wells is approximately 1000 m. During the detection process, the current injected into the downhole electrode diffuses into the formation with spherical symmetry. When a low-resistance body, such as copper ore, with a much higher conductivity than that of the formation is encountered, the current converges around it to generate a low-frequency alternating magnetic field that contains the conductivity information of the strata. Then, the magnetic field is sensed by the receiving probe for further analysis to obtain the distribution of the low-resistance body.

Since the downhole electrode operates in the well at a depth of hundreds or even thousands of meters, far from the surface, the response of the system model can be considered a whole-space problem. Assuming that the surface electrode is located at an infinite distance and that the borehole size is much smaller than the well spacing, the downhole electrode can be considered a point current source [39]. Consider a column coordinate system in an infinite homogeneous formation, assuming that the spatial position of the transmitting electrode is (ρ_0, φ_0, z_0); then, the electric field intensity at any point $P(\rho, \varphi, z)$ in the space is [40]

$$E = \frac{I_j}{4\pi\sigma_e R^2},\tag{1}$$

where σ_e denotes the conductivity of the formation, I_j represents the current injected into the transmitting electrode, and $R = [(\rho - \rho_0)^2 + (\varphi - \varphi_0)^2 + (z - z_0)^2]^{1/2}$ represents the field source distance. Based on the electric field equation, the magnetic field at any point in space can be further calculated by using the classical formulas of electromagnetism. From (1), we can see that a large injection current could enhance the field, which is conducive to achieving long-distance detection. In addition, frequency, which is another important parameter, also affects detection performance. To avoid 50-Hz industrial frequency interference, a frequency of 15.625 Hz is selected for subsequent study in this article.

The traditional numerical calculation method as shown in (1) can theoretically characterize the feasibility of the method proposed in this article; however, it cannot accurately reflect the actual complex stratum structure. Specifically, the shape of a metal anomaly is not necessarily a regular column, which may cause a significant deviation between the calculation results and actual values. In addition, the model structure becomes very complex when there are many low-resistance bodies in the formation, which leads to difficulty in obtaining an accurate analytical solution. To improve the detection accuracy of metal ores, we use the finite-element method (FEM) to simulate and analyze the response of the system model of irregular and multiple low-resistance bodies.

III. IRREGULAR MULTIANOMALY MODEL IN THE CROSSWELL SYSTEM

In this article, the structure of two real copper ores in Daye City, China, is considered for our simulation, where prior knowledge is obtained from numerous well-logging responses that indicate that there are two irregular copper ores in the stratum, located at a depth of approximately 750 and 1000 m, respectively.
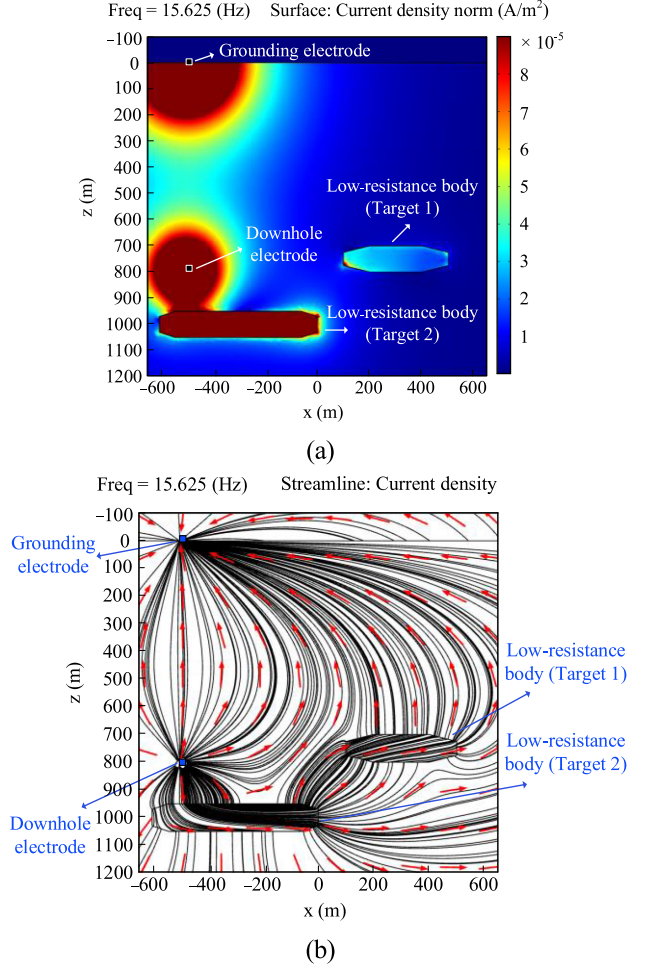

Fig. 2. Current distribution of the detection area. (a) Current density distribution. (b) Current streamline chart.

Based on the above-mentioned information, a two-dimensional (2-D) FEM model containing multiple anomalies is established to characterize the EM response on the profile (*x-z* plane) consisting of the two well axes. Specifically, a scene consisting of a source with 3-D properties and a geophysical model with 2-D characteristics may also be referred to as 2.5-D, which is realized by performing a spatial Fourier transform in one of the horizontal directions and solving Maxwell's/Helmholtz equations to obtain the wavenumber domain field, then the (x, y, z) domain EM fields could be obtained by performing an inversion Fourier transform [41]. In our model, the *x*-axis represents the position in the horizontal direction, while the *z*-axis represents the depth position along the well axis. We assume that the area from $z = -100$ m to $z = 0$ m is the air layer and that the area from $z = 0$ m to $z = 1200$ m is the stratum. The transmitter well is located at $x = -500$ m, and the receiver well is located at $x = 500$ m.

The current density distribution in the formation between the two wells is presented in Fig. 2(a) when the transmitting electrode is located at $x = -500$ m and $z = 800$ m, and the grounding electrode is located at $x = -500$ m and $z = 0$ m. The figure demonstrates that the current density of the two
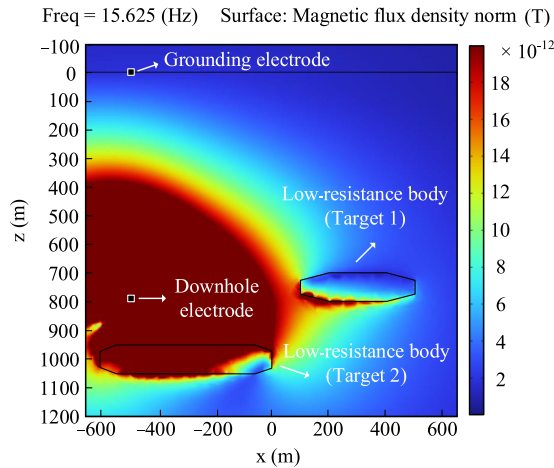
Fig. 3.   Magnetic field distribution.

low-resistance bodies is significantly higher than that of other areas in the formation, which indicates that the low-resistance bodies converge the currents. In Fig. 2(b), a current streamline chart is presented to further clarify the transmission mechanism. The figure demonstrates that the currents start from the transmitting electrode and flow to the grounding electrode with a lower potential. The currents change direction and converge when encountering low-resistance anomalies. According to this phenomenon, we infer that the converging currents may generate magnetic fields, which would make the magnetic field distribution in the research area containing anomalies different from that of a homogeneous stratum without anomalies. To verify the reliability of our inference, we simulate the magnetic field distribution in the target region. As shown in Fig. 3, the magnetic field gradually decays as the propagation distance increases. However, it is noteworthy that the magnetic fields in the partial region at the edges (or surfaces) of the two anomalies are significantly stronger than that in the surrounding area. By combining the distribution characteristics of the current density mentioned earlier, we could attribute this phenomenon to the magnetic field generated by the converging currents of the anomalies.

During the detection process, we expect to acquire EM signals containing different stratigraphic information by moving the transmitter and receiver to different depth positions, thus obtaining the conductivity distribution of the whole area. Therefore, we simulate the values of current density and magnetic flux density at different probing sites [as shown in Fig. 4(a) and (b)]. Moreover, in order to demonstrate the effect of low-resistance bodies on the received signals more intuitively, we complete the above-mentioned simulations for two cases: with and without low-resistance bodies. Fig. 4(a) demonstrates that the current density of the received signal between 700 and 800 m downhole is greater when there are low-resistance bodies in the formation than when there are no anomalies, and the positions of the abnormalities are related to the locations of the low-resistance bodies. In addition, during the process of moving the transmitter from 900 to 700 m, the value of the corresponding current density decreases overall as the transmitter gradually moves away from the deeper low-resistance body, which indicates
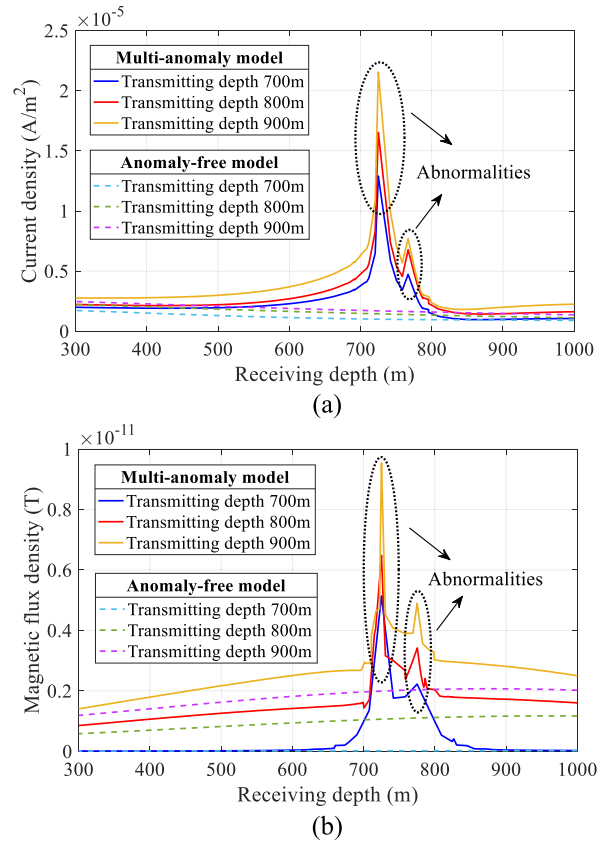
Fig. 4.   Comparison of responses under different geological conditions. (a) Current density. (b) Magnetic flux density.

that the current convergence capacity decreases with an increasing distance between the transmitting electrode and the low-resistance body. The magnetic flux density in the same case is presented in Fig. 4(b). Similarly, between 700 and 800 m, the responses of the multianomaly model are significantly stronger than the responses of the anomaly free model at the corresponding detection site. Therefore, low-resistance bodies can effectively converge the current and generate a low-frequency alternating magnetic field, thus enhancing the received magnetic field and facilitating reliable detection. In addition, we can see that the deeper the transmitting electrode, the greater the value of magnetic flux density for the abnormalities. By utilizing the differences between the responses at different detection locations, we can obtain information about the objective area, and the distribution of low-resistance bodies can be determined by processing and interpreting the received signals.

IV. DESIGN OF GROUNDING ELECTRODE PLACEMENT SCHEME

Based on the discussion in Section III, we can see that abnormalities in the received signal reflect the number of low-resistance bodies, and the distribution of the low-resistance bodies can be determined by interpreting the data. However, under the parameters set in Section III, the received magnetic field is altered when the transmitting electrode position changes, which indicates that movement of the transmitting electrode affects the detection performance. In fact, in addition to the
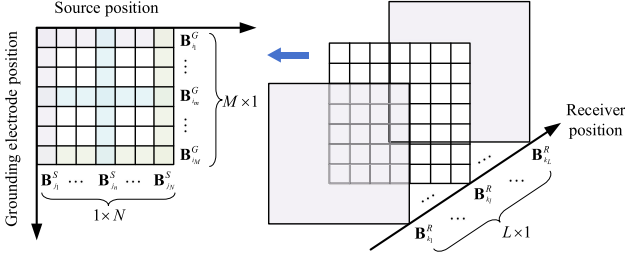
Fig. 5. Problem space for crosswell EM dataset.

current and frequency, which are analyzed in Section II, factors such as the positions of the transmitting electrode, grounding electrode, and receiving magnetic probe may also affect the detection performance. To improve the detection performance, this section analyzes these factors by constructing a crosswell EM dataset model, and designs a placement scheme for the grounding electrode.

A. Dataset Model for Crosswell EM Logging

To describe the design process of the grounding electrode placement scheme more thoroughly, we build a problem space for the dataset. Suppose that the transmitting electrode moves to N different positions to transmit signals ($n = 1, \ldots, N$, from bottom to top of the transmitter well), and that the magnetic probe has a total of L different receiving positions ($l = 1, \ldots, L$, from bottom to top of the receiver well). In addition, the grounding electrode is placed at M different positions ($m = 1, \ldots, M$, from left to right) on the surface between the transmitter well and receiver well. Then, the dataset can be represented as a special problem space illustrated in Fig. 5.

In this model, the magnetic field with grounding electrode position i_m, transmitting position j_n, and receiving position k_l is represented as b_{i_m,j_n,k_l}. Therefore, for any specific receiving position k_l, the spatial problem can be simplified as a 2-D problem, and its row and column vectors can be expressed as follows:

$$\mathbf{B}_{i_m}^G = [b_{i_m,j_1,k_l}, \cdots, b_{i_m,j_n,k_l}, \cdots, b_{i_m,j_N,k_l}]_{1 \times N} \quad (2)$$

$$\mathbf{B}_{j_n}^S = [b_{i_1,j_n,k_l}, \cdots, b_{i_m,j_n,k_l}, \cdots, b_{i_M,j_n,k_l}]_{M \times 1}^T \quad (3)$$

respectively, where $\boldsymbol{B}_{i_m}^G$ represents the received magnetic field when the transmitting electrode moves in N different positions while the grounding electrode is fixed at position i_m. Similarly, $\boldsymbol{B}_{j_n}^S$ represents the received magnetic field when the grounding electrode moves in M different positions while the transmitting electrode is fixed at position j_n. Therefore, the magnetic field under different placement schemes corresponding to a specific receiving position k_l can be expressed as follows:

$$\mathbf{B}_{k_l}^R = \left[\mathbf{B}_{j_1}^S, \cdots, \mathbf{B}_{j_n}^S, \cdots, \mathbf{B}_{j_N}^S \right]_{M \times N}$$

$$= \begin{bmatrix} b_{i_1,j_1,k_l} & \cdots & b_{i_1,j_n,k_l} & \cdots & b_{i_1,j_N,k_l} \\ \vdots & \vdots & \vdots & \vdots & \vdots \\ b_{i_m,j_1,k_l} & \cdots & b_{i_m,j_n,k_l} & \cdots & b_{i_m,j_N,k_l} \\ \vdots & \vdots & \vdots & \vdots & \vdots \\ b_{i_M,j_1,k_l} & \cdots & b_{i_M,j_n,k_l} & \cdots & b_{i_M,j_N,k_l} \end{bmatrix}_{M \times N}. \quad (4)$$
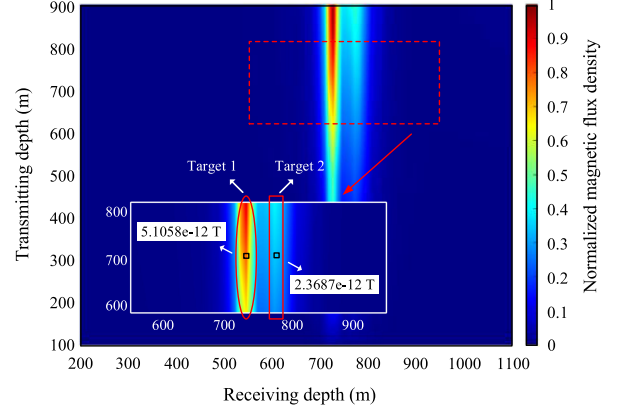
(a)
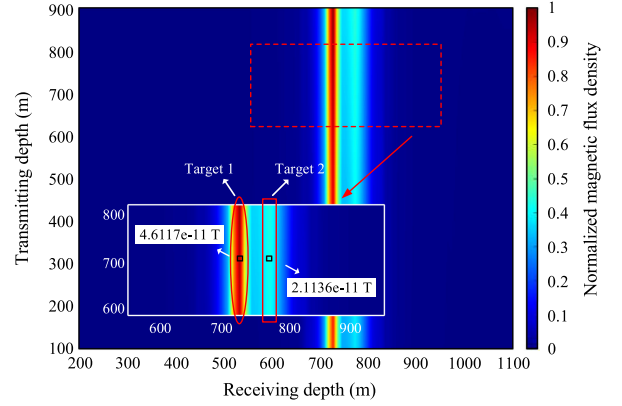
(b)

Fig. 6. Normalized magnetic field distribution. (a) Grounding electrode is placed at the transmitting wellhead. (b) Grounding electrode is placed at the receiving wellhead.

Then, the simulation data of the magnetic field in the entire problem space can be expressed as follows:

$$\mathbf{B}^{sim} = \{\mathbf{B}_{k_1}^R, \cdots, \mathbf{B}_{k_l}^R, \cdots, \mathbf{B}_{k_L}^R\}_{M \times N \times L}. \quad (5)$$

B. Performance Analysis of Grounding Electrode Placement Scheme

Based on the crosswell EM dataset model constructed in Section IV-A, the distribution of the magnetic field in the receiver well corresponding to different transmitting positions is simulated when the grounding electrode is placed at the transmitting wellhead ($i_1 = -500$ m) and the receiving wellhead ($i_2 = 500$ m), respectively [Fig. 6(a) and (b)].

Comparing the normalized magnetic field distributions in Fig. 6(a) and (b), we can see that they both reflect the presence of two low-resistance targets; however, the effect of the transmitting position on the magnetic field distribution is different under the two placement schemes. In Fig. 6(a), when the transmitting electrode moves up from the bottom of the transmitter well, the magnetic field at each position in the receiver well is correspondingly reduced; that is, for any receiving position k_l, we have $b_{i_1, j_1, kl} > b_{i_1, j_2, kl} > \ldots > b_{i_1, j_N, kl}$. However, in Fig. 6(b), there is no significant difference in the received magnetic field as the transmitting electrode moves; that is, $b_{i_2, j_1, kl} \approx b_{i_2, j_2, kl} \approx \ldots \approx b_{i_2, j_N, kl}$. This observation demonstrates that
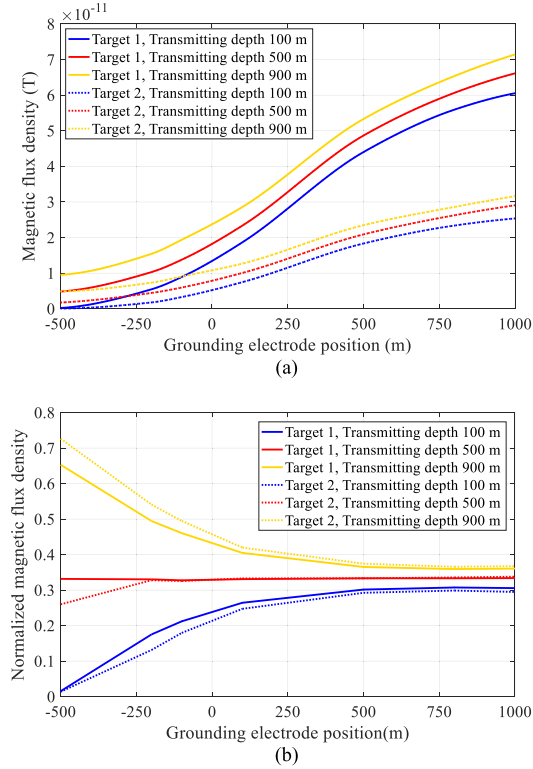
Fig. 7. Change in magnetic flux density under different grounding electrode placement schemes. (a) Original graph. (b) Normalized graph.

when the grounding electrode is placed at different positions, the distribution of the magnetic field is affected differently by the transmitting position. In the case illustrated in Fig. 6(b), a dataset consisting of elements with similar values may causes large fluctuations in the initial stage of the inversion and impedes the inversion process. Therefore, the placement of the grounding electrode affects the detection performance. To obtain the optimal placement scheme for improved detection, we further study how the received magnetic field changes with the movement of the grounding electrode. Fig. 6(a) and (b) indicate that when the transmitting electrode moves, the magnetic field does not change significantly at any receiving position except for the positions corresponding to the magnetic anomalies; therefore, we simplify the dimension of the receiving position by selecting only two depth positions, $k_1 = 726$ m and $k_2 = 776$ m, corresponding to the two magnetic anomalies. The magnetic field distribution is simulated when the grounding electrode is placed in different horizontal positions, and the results are presented in Fig. 7.

It can be seen that the results presented in Fig. 7(a) and (b) are somewhat contradictory. Fig. 7(a) indicates that the magnetic fields at both magnetic anomaly positions increase gradually with the horizontal distance of the grounding electrode; that is, for any transmitting position j_n, we have $b_{i1, jn, k1} < \ldots < b_{im, jn, k1} < \ldots < b_{iM, jn, k1}$ and $b_{i1, jn, k2} < \ldots < b_{im, jn, k2} < \ldots < b_{iM, jn, k2}$. This suggests that more current is forced to pass through low-resistance bodies in the formation to reach the grounding electrode when the grounding electrode is placed farther away, which increases the signal strength of the anomaly

response in the receiver well and thus facilitates crosswell EM detection. To further evaluate the effect of the change in the transmitting position on the two magnetic anomaly responses under different grounding electrode placement schemes, we normalize the magnetic field values corresponding to the three different transmitting positions in Fig. 7(a) for each grounding electrode placement scenario, as illustrated in Fig. 7(b). We can see that for all magnetic anomalies, when the grounding electrode is moved far away, the differences between the magnetic fields generated by different transmitting positions in the receiver well decrease. When the grounding electrode is placed around the receiving wellhead even farther away ($i_m \geq 500$ m), the movement of the transmitting electrode hardly affects the received signal. This result indicates that when the grounding electrode is far away, the path length of the injected current from the transmitting electrode to the grounding electrode along different paths is approximately the same. Since the electrical conductivity of the anomalies is much greater than that of the formation, the current always flows along an almost identical path, that is, through low-resistance bodies to the grounding electrode. Considering the instability of the inversion process, it can be seen that placing the grounding electrode at a far distance from the transmitter well is not conducive to the interpretation of the stratum distribution and may cause significant errors or even infinitely many solutions in the inversion.

According to the above-mentioned analysis, it is desirable to place the grounding electrode close to the transmitter well under the condition that the signal strength is sufficient. This allows the flow paths of the injected current at different positions in the transmitter well to be as different as possible, which can help obtain more information for better inversion of the stratigraphic distribution. As can be seen from Fig. 6(a), when the grounding electrode is placed near the transmitter well, if the transmitting position is deeper than 700 m, the magnetic field values of the two abnormal positions in the receiver well reach the order of 10^{-12} T, which can be detected by a high-sensitivity magnetic probe. Therefore, for the multitarget model proposed in this article, if the transmitting electrode moves in an area deeper than 700 m downhole, placing the grounding electrode at the transmitting wellhead leads to optimal detection performance.

V. FIELD MEASUREMENTS

Based on the above-mentioned research results, relevant field measurements were performed in Daye City, China. As illustrated in Fig. 8, two wells were drilled for the experiment according to the 2-D FEM model. Both of them were nearly vertical, thus making the experimental environment fit the model as closely as possible. The transmitter well, zk40910, and receiver well, zk409, were more than 1000 m deep and approximately 1000 m apart, and the grounding electrode was placed near the transmitter well. According to the analysis in Section II, the operating frequency was set to 15.625 Hz. Prior logging information indicated that both copper ores located in the stratum were close to the wellbores, which was favorable for the convergence of the injected current. Based on this information, we adopted an ac of 30 A for excitation in consideration of cost constraints. Due
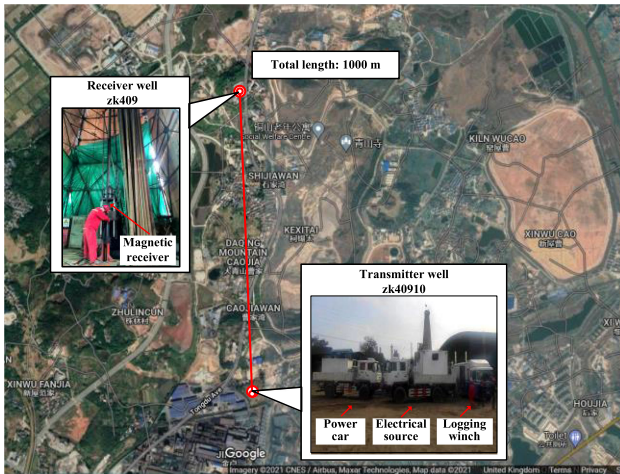
Fig. 8. Field test with wells spaced approximately 1000 m apart.

Fig. 9. Schematic diagram of the test process and part of the raw data.

Fig. 10. Comparison between measured data and simulation results.

to the large well spacing, a highly sensitive magnetic probe was used to receive the signal. Considering the limited space of the borehole with a diameter of 50 mm, we designed the transmitting electrode with a diameter of 30 mm and a length of 1.6 m, and the receiving probe with an outside diameter of 30 mm and the length of 3.6 m. Specifically, the receiver was connected to the circuit by three coils in series with a total number of turns of 75000. To achieve long-distance detection, we selected the 1J85 Permalloy as the material of the core for the magnetic probe to enhance the strength of EM signals [42].

In our experiments, considering the bearing strength and heat resistance characteristics of the downhole instruments, we combined prior knowledge of the anomaly distribution and selected an area of 700–1000 m downhole for detection. During the test, the transmitter moved between 700 and 1000 m in well zk40910, and the receiver moved within the same depth range in well zk409 to obtain EM signals under different paths. The surface system was used to process the received signals, and the synchronization between the receiver and the transmitter was achieved based on GPS receivers to ensure reliable communication. The entire test process contained several transmitter and receiver positions at depth intervals equal to 10 m. The measurement process and part of the raw data are presented in Fig. 9.

To examine the correspondence between the measured and simulation data, we selected a segment of the raw data of the entire receiving area when the transmitter was lowered 700 m downhole for processing. We divided the raw data presented in Fig. 9 by the receiver pregain and performed filtering and denoising to obtain the measured data presented in Fig. 10. It can be seen that the simulation and measurement results exhibited the same trend, and both reflected the magnetic anomalies caused by the two low-resistance bodies in the formation. However, due to the complexity of the actual stratum structure, there was a discrepancy between the measurement data and simulation data. The detection results were also affected by the uncertainty of the shape and properties of the low-resistance bodies, which resulted in the inaccurate correspondence between the measured and simulated anomaly positions.
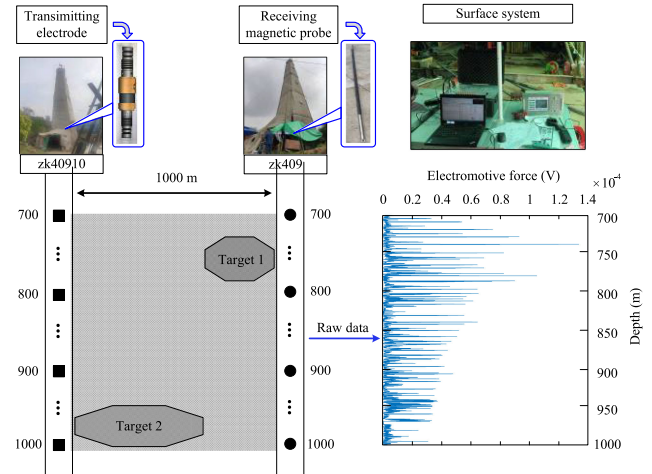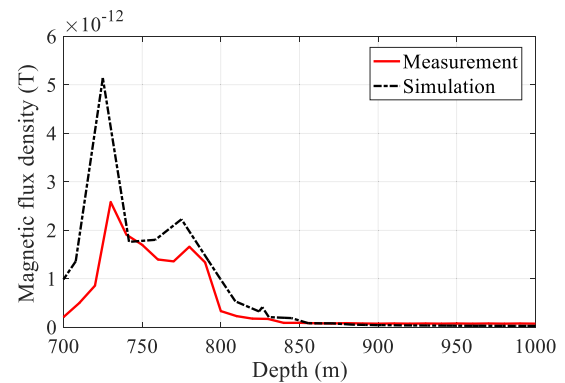
Relevant simulation results in Sections III and IV indicate that the EM signals reach the receiver via different transmission paths, so they carry different information about the conductivity associated with the stratum. Therefore, we could obtain the conductivity information for the entire detection area corresponding to the 2-D FEM model by interpreting these signals. There are many developed inversion algorithms for data interpretation, such as the iterative Born inversion technique [43]–[45], the distorted Born iterative method [46], and the Newton iterative method [5], etc. In addition, there is still a great platform named MARE2DEM for high-precision forward modeling and inversion, which could be applied to multiple geophysical scenes with 2.5-D interpretation [47]. Since the main contribution of this study is the extension of existing theories for long-distance crosswell application without the innovation of the interpretation method, we adopt the classical Gauss-Newton method [48] to perform the inversion. It is known that the Gauss-Newton method is a traditional nonlinear iterative method that can perform well in image interpretation in the field of geophysics. Taking advantage of the fast imaging and small error of this classical inversion algorithm, we interpret the measured dataset acquired in the particular environment to evaluate the detection results more intuitively. The general inversion problem can be

expressed as follows:

$$\min \quad \mathbf{P}^\lambda(\mathbf{m}) = \left\| \mathbf{W}_d [\mathbf{d}^{obs} - \mathbf{F}(\mathbf{m})] \right\|^2$$
$$+ \lambda \left\| \mathbf{W}_m [\mathbf{m} - \mathbf{m}^{ref}] \right\|^2. \tag{6}$$

In (6), the first term on the right is a measure of data misfit and denotes a norm of the weighted difference between the observed data $\mathbf{d}^{obs}$ and the theoretical values $\mathbf{F}(\mathbf{m})$; the second term is the regularization term, consisting of a stabilizer and the regularization factor λ used to prevent the overfitting of the data. $\mathbf{P}^\lambda(\mathbf{m})$ is the objective function, $\mathbf{m}^{ref}$ represents the known prior model, and $\mathbf{m}$ represents the unknown inversion model. Specifically, we have $\mathbf{m} = \text{vec}(\sigma)$ and $\sigma = [\sigma(x_u, z_v), u = 1, ..., U; v = 1, ..., V]$. Each element $\sigma(x_u, z_v)$ of the matrix σ represents the electrical conductivity at the corresponding location, where x_u and z_v describe the central position of each 2-D discretization cell resulting from the grid partitioning of the entire target region (x-z plane) in the forward process, and U and V denote the number of cells that the model is discretized along the x-direction and z-direction, respectively. $\mathbf{W}_d$ and $\mathbf{W}_m$ are the weighting matrices of the measured data and the model, respectively. During the inversion process, $\mathbf{W}_d$ allows us to set the variance for each datum to its appropriate level and $\mathbf{W}_m$ controls the closeness between the inverted model $\mathbf{m}$ and reference model $\mathbf{m}^{ref}$. The choice of $\mathbf{W}_d$ and $\mathbf{W}_m$ has a great influence on the inversion result. Advanced parameter estimation and optimization methods can help us obtain high-precision imaging results [49]–[51]. Here, in order to reduce the complexity of the subsequent interpretation, we assume that the data are independent of each other and all follow a Gaussian distribution. Then, $\mathbf{W}_d$ is an $NL \times NL$ diagonal matrix whose elements are the reciprocal of the standard deviations of the noise. For example, $\mathbf{W}_d = \text{diag}(\varepsilon_1, ..., \varepsilon_{nl}, ..., \varepsilon_{NL})^{-1}$, where ε_{nl} is the uncertainty of the nlth datum. Similarly, $\mathbf{W}_m$ is a $UV \times UV$ diagonal matrix as $\mathbf{W}_m = \text{diag}(\gamma_1, ..., \gamma_{uv}, ..., \gamma_{UV})^{-1}$, where γ_{uv} is the standard deviation of the uvth model component.

In the initial steps of the inversion, the value of the first term in (6) is relatively large; therefore, a large value of $\mathbf{W}_d$ is required to reduce the effect of the regular term and thus determine the optimal search direction. Using the Taylor expansion of $\mathbf{F}(\mathbf{m})$, the objective function can be represented as follows:

$$\min \quad \mathbf{P}^\lambda(\mathbf{m}^k) = \left\| \mathbf{W}_d [\mathbf{d}^{obs} - \mathbf{d}^k - \mathbf{J}^k \Delta\mathbf{m}] \right\|^2$$
$$+ \lambda \left\| \mathbf{W}_m [\mathbf{m}^k - \mathbf{m}^{ref}] \right\|^2 \tag{7}$$

where $\mathbf{J}^k$ is the Jacobian matrix, $\mathbf{m}^{k+1}$ is the result of the $k+1$th iteration, and $\mathbf{d}^k = \mathbf{F}(\mathbf{m}^k)$ is the result of the kth forward modeling. Solving the minimization problem of (7), we obtain the following:

$$\Delta\mathbf{m} = \left(\mathbf{J}^{k^T} \mathbf{W}_d^T \mathbf{W}_d \mathbf{J}^k + \lambda \mathbf{W}_m^T \mathbf{W}_m \right)^{-1}$$
$$\cdot \left\{ \mathbf{J}^{k^T} \mathbf{W}_d^T \mathbf{W}_d [\mathbf{d}^{obs} - \mathbf{d}^k] - \lambda \mathbf{W}_m^T \mathbf{W}_m [\mathbf{m}^k - \mathbf{m}^{ref}] \right\}. \tag{8}$$

Based on $\Delta\mathbf{m}$, the unknown model of the next iteration can be updated as $\mathbf{m}^{k+1} = \mathbf{m}^k + \Delta\mathbf{m}$ until $\Delta\mathbf{m}$ or $\mathbf{F}(\mathbf{m}^k)$-$\mathbf{F}(\mathbf{m}^{k-1})$ is sufficiently small; then, $\mathbf{m}$ of the last iteration is considered the final inversion result.
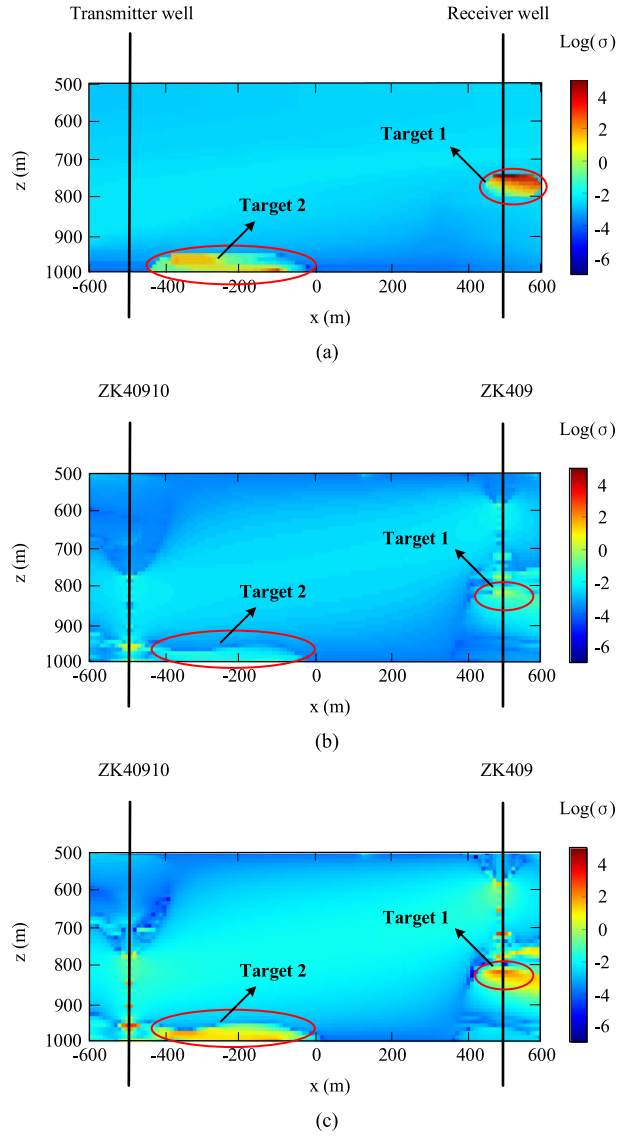

Fig. 11. Inversion results. (a) Inversion result based on simulation data. (b) Inversion result based on measured data after three iterations. (c) Inversion result based on measured data after five iterations.

According to the above-mentioned Gauss–Newton method, we first complete the interpretation for simulated data to verify the reliability of the inversion algorithm before the inversion of the measured data. Specifically, we obtained simulated dataset using the 2-D FEM model described in Section III and interpreted it using the constructed algorithm. Fig. 11(a) presents the inversion results based on the simulation data obtained by placing the grounding electrode at the transmitting wellhead, and the results illustrate that the distribution of anomalies is consistent with prior knowledge. Compared with the simulation model constructed in Section III, the depth positions of both anomalies are accurately reflected; however, there are small deviations in their horizontal positions and sizes, which may be caused by the influence of the model boundary conditions and the limitations of the algorithm accuracy. We are performing related research and will present high-precision interpretation results in our subsequent work.

Given the above-mentioned result, we consider that such an interpretation is reliable and can provide us with the information necessary to verify the validity of the detection method proposed in this article for new applications. In order to characterize the imaging process for measured data more directly, we give the following imaging results with different number of iterations. Fig. 11(b) represents the imaging result for measured data after three iterations. It can be seen that the conductivity of the research area exhibits partial differences [especially with respect to the conductivity values of the area corresponding to the targets in Fig. 11(a)]. However, the difference in conductivity between the targets and the surrounding environment is not very large, and it does not clearly characterize the features of the ore bodies. In addition, the edges of the targets in this figure are very blurred, making it difficult to form a valid comparison with the prior information. Fig. 11(c) presents the inversion result obtained by iterating five times with the measured data. The figure demonstrates that there are two low-resistance anomalies in the formation, located in regions 950–1000 m and 750–850 m downhole, which is comparable to the simulation results. However, there are several bright spots along two wellbores ($x = -500$ m and $x = 500$ m) in Fig. 11(c), which may be caused by noise generated during the movement of the transmitter and receiver. In addition, affected by the complex wellbore structure, the quality of the data around the two wells is not very good, resulting in a nonuniform conductivity distribution. Although the imaging results displayed in Fig. 11(c) are not as favorable as those in Fig. 11(a), they nevertheless present the distribution of low-resistance bodies similar to the prior information. Furthermore, because the actual size and shape of the anomalies are somewhat different from those in the simulation model, the positions of the anomalies presented in Fig. 11(c) are also somewhat different from those in Fig. 11(a), which is consistent with the differences presented in Fig. 10.

Based on the above-mentioned discussion, the detection method proposed in this article can use only two wells to determine the distribution of low-resistance anomalies described by prior information obtained from numerous well logging, which is of great importance to save detection costs and improve detection efficiency. It should be clarified that the modeling and inversion are currently performed based on traditional algorithms, but the interpretation results can still provide a reliable basis for the feasibility of the proposed method. In the future, we will adopt advanced platform [46] and optimization algorithms [48]–[50] to realize more valuable data interpretation, and the study of high-precision inversion will be presented as our subsequent work.

VI. CONCLUSION

Given the borehole size limitation of wells used for copper ore exploration and the short detection distance caused by the rapid attenuation of EM waves in a low-resistance environment, this article proposes a crosswell EM logging method based on the borehole-surface current injection technique. This study uses low-resistance bodies in the formation to converge the current, thereby generating a low-frequency alternating magnetic field received by a high-sensitivity magnetic probe to achieve long-distance detection. Based on a series of modeling and simulations, we conducted large-scale field experiments with two slim open holes spaced approximately 1000 m apart and interpreted the measured data. The results indicated that the distribution of both low-resistance anomalies was in good agreement with prior logging information obtained from numerous well loggings, thus verifying the effectiveness of the crosswell application described in this article.

In conclusion, such an extended application of classical theories demonstrates the probability of solving the problem for long-distance detection in slim open holes and also reduce the complexity of the experiment by using only two wells instead of numerous wells to obtain information, which could make the crosswell EM logging more convenient and thus further promote the practical application of such tools and methods.

REFERENCES

[1] L. Wang, S. Li, and Y. Fan, "An all-new ultradeep detection method based on hybrid dipole antennas in electromagnetic logging while drilling," *IEEE Trans. Geosci. Remote Sens.*, vol. 58, no. 3, pp. 2124–2134, Mar. 2020.

[2] Z. Jiang, S. C. Liu, and R. Malekian, "Analysis of a whole-space transient electromagnetic field in 2.5-dimensional FDTD geoelectric modeling," *IEEE Access*, vol. 5, pp. 18707–18714, 2017.

[3] J. Chang, J. Yu, J. Li, G. Xue, R. Malekian, and B. Su, "Diffusion law of whole-space transient electromagnetic field generated by the underground magnetic source and its application," *IEEE Access*, vol. 7, pp. 63415–63425, 2019.

[4] Z. Jiang, L. Liu, S. Liu, and J. Yue, "Surface-to-underground transient electromagnetic detection of water-bearing goaves," *IEEE Trans. Geosci. Remote Sens.*, vol. 57, no. 8, pp. 5303–5318, Aug. 2019.

[5] A. Abubakar, T. M. Habashy, V. L. Druskin, L. Knizhnerman, and D. Alumbaugh, "2.5D forward and inverse modeling for the interpretation of low-frequency electromagnetic measurements," *Geophysics*, vol. 73, no. 4, pp. F165–F177, Aug. 2008.

[6] D. L. Alumbaugh *et al.*, "Multi-scale data integration in crosswell EM imaging and interpretation," in *Proc. Soc. Exploration Geophys. Int. Expo. Annu. Meeting.*, 2008, pp. 3541–3544.

[7] T. Patzek, M. Wilt, and G. M. Hoversten, "Using electromagnetics (EM) for reservoir characterization and waterflood monitoring," in *Proc. Permian Basin Oil Gas Rec. Conf.*, 2000, pp. 1–8.

[8] M. L. Sanni, N. Yeh, N. I. Afaleg, and A. Ai-Kaabi, "Crosswell electromagnetic resistivity tomography: Pushing and limits," in *Proc. SPE Middle East Oil Gas Show Conf.*, 2007, pp. 955–959.

[9] Z. Yang, Y. Ji, Z. Li, H. Wang, and F. Guo, "A fast forward and inversion method for long distance cross-well electromagnetic imaging logging system," in *Proc. Photon. Electromagn. Res. Symp.*, 2019, pp. 2369–2378.

[10] G. M. Hoversten, G. A. Newman, H. F. Morrison, E. Gasperikova, and J. Berg, "Reservoir characterization using crosswell electromagnetic inversion: A feasibility study for the Snorre field, north sea," *Geophysics*, vol. 66, no. 4, pp. 1177–1189, Aug. 2001.

[11] M. Wilt, P. Zhang, and M. Safdar, "Crosswell electromagnetic tomography in unconventional well geometries," in *Proc. SPE Annu. Tech. Conf. Exhib.*, 2011, pp. 3629–3634.

[12] Z. Yu, J. Zhou, Y. Fang, Y. Hu, and Q. H. Liu, "Through-casing hydraulic fracture evaluation by induction logging II: The inversion algorithm and experimental validations," *IEEE Trans. Geosci. Remote Sens.*, vol. 55, no. 2, pp. 1189–1198, Feb. 2017.

[13] D. Denney, "Crosswell technologies: New solutions for enhanced reservoir surveillance," *J. Petroleum Technol.*, vol. 63, no. 9, pp. 56–58, Jul. 2011.

[14] J. M. Donadille and S. M. Al-Ofi, "Crosswell electromagnetic response in a fractured medium," *Geophysics*, vol. 77, no. 3, pp. D53–D61, Jun. 2012.

[15] M. Wilt *et al.*, "Crosshole electromagnetic tomography: A new technology for oil field characterization," *Leading Edge*, vol. 14, no. 3, pp. 173–177, Mar. 1999.

[16] K. Maclennan, M. Karaoulis, and A. Revil, "Complex conductivity tomography using low-frequency crosswell electromagnetic data," *Geophysics*, vol. 79, no. 1, pp. E23–E38, Feb. 2014.

[17] Y. Zhou, L. Shi, N. Liu, C. Zhu, Y. Sun, and Q. H. Liu, "Mixed spectral-element method for overcoming the low-frequency breakdown problem in subsurface EM exploration," *IEEE Trans. Geosci. Remote Sens.*, vol. 55, no. 6, pp. 3488–3500, Jun. 2017.

[18] M. J. Wilt, D. L. Alumbaugh, H. F. Morrison, A. Becker, K. H. Lee, and M. Deszcz-Pan, "Crosswell electromagnetic tomography: System design considerations and field results," *Geophysics*, vol. 60, no. 3, pp. 871–885, Jun. 1995.

[19] M. J. Wilt and D. L. Alumbaugh, "Oil field reservoir characterization and monitoring using electromagnetic geophysical techniques," *J. Petroleum Sci. Eng.*, vol. 39, no. 1, pp. 85–97, Aug. 2003.

[20] K. Zhou, J. Tao, D. Mo, Y. Han, and Y. Duan, "Precision timing synchronization in crosswell electromagnetic logging tool," in *Proc. Chin. Autom. Congr.*, 2015, pp. 1069–1074.

[21] D. L. Alumbaugh and H. F. Morrison, "Theoretical and practical considerations for crosswell electromagnetic tomography assuming a cylindrical geometry," *Geophysics*, vol. 60, no. 3, pp. 846–870, Jun. 1995.

[22] L. DePavia *et al.*, "Next generation crosswell EM imaging tool," in *Proc. SPE Annu. Tech. Conf. Exhib.*, 2008, pp. 3890–3900.

[23] A. Moschitta, A. De Angelis, F. Santoni, M. Dionigi, P. Carbone, and G. De Angelis, "Estimation of the magnetic dipole moment of a coil using AC voltage measurements," *IEEE Trans. Instrum. Meas.*, vol. 67, no. 10, pp. 2495–2503, Oct. 2018.

[24] B. R. Spies, "Depth of investigation in electromagnetic sounding methods," *Geophysics*, vol. 54, no. 7, pp. 872–888, Jul. 1989.

[25] K. M. Strack, *Exploration With Deep Transient Electromagnetic Method*. New York, NY, USA: Elsevier, 1992, pp. 1–373.

[26] W. Xie, X. Zhang, Y. Zheng, and Y. Mu, "A fast 3D imaging method for subsurface metal targets using time-domain electromagnetic device," in *Proc. Dig. Int. Geosci. Remote Sens. Symp.*, 2019, pp. 9992–9994.

[27] D. Alumbaugh and E. Um, *On the Physics of Galvanic Source Electromagnetic Geophysical Methods for Terrestrial and Marine Exploration*. Madison, WI, USA: Univ. Wisconsin–Madison, 2007, pp. 5–9.

[28] N. Zhou *et al.*, "A comparison of different-mode fields generated from grounded-wire source based on the 1D model," *Pure Appl. Geophys.*, vol. 173, no. 2, pp. 591–606, 2016.

[29] A. A. Kaufman and G. V. Keller, *Frequency and Transient Soundings*. Amsterdam, The Netherlands: Elsevier, 1983, pp. 213–411.

[30] L. Yu and R. N. Edwards, "On crosswell diffusive time-domain electromagnetic tomography," *Geophys. J. Int.*, vol. 130, no. 2, pp. 449–459, Apr. 1997.

[31] G. Xue, W. Chen, and S. Yan, "Research study on the short offset time-domain electromagnetic method for deep exploration," *J. Appl. Geophys.*, vol. 155, pp. 131–137, Jun. 2018.

[32] T. Uchida, K. H. Lee, and M. J. Wilt, "Effect of a steel casing on crosshole EM measurement," in *Proc. SEG Annu. Meeting*, 1996, pp. 230–233.

[33] D. Pardo, C. Torres-Verdín, and Z. Zhang, "Sensitivity study of borehole-to-surface and crosswell electromagnetic measurements acquired with energized steel casing to water displacement in hydrocarbon-bearing layers," *Geophysics*, vol. 73, no. 6, pp. F261–F268, Dec. 2008.

[34] M. Commer, G. M. Hoversten, and E. S. Um, "Transient-electromagnetic finite-difference time-domain earth modeling over steel infrastructure," *Geophysics*, vol. 80, no. 2, pp. E147–E162, Apr. 2015.

[35] A. F. Kuckes, T. Lautzenhiser, A. G. Nekut, and R. Sigal, "An electromagnetic survey method for directionally drilling a relief well into a blown out oil or gas well," *Soc. Petroleum Eng. J.*, vol. 24, no. 3, pp. 269–274, Jun. 1984.

[36] Z. He, X. Liu, W. Qiu, and H. Zhou, "Mapping reservoir boundary by borehole-surface TFEM: Two case studies," *Geophysics*, vol. 24, no. 9, pp. 896–900, Sep. 2005.

[37] Y. Hu, Y. Fang, D. LaBrecque, M. Ahmadian, and Q. H. Liu, "Reconstruction of high-contrast proppant in hydraulic fractures with galvanic measurements," *IEEE Trans. Geosci. Remote Sens.*, vol. 56, no. 4, pp. 2066–2073, Apr. 2018.

[38] A. D. Hibbs *et al.*, "Advances in electromagnetic survey instrumentation and the use of a cased borehole for imaging a deep formations," in *Proc. EAGE Conf. Exhib.*, 2014, pp. 253–255.

[39] J. Xu, *Electromagnetic Field and Electromagnetic Wave in Layered Media*. Beijing, China: Petroleum Industry, 1997, pp. 1–244.

[40] A. A. Kaufman and Y. A. Dashevsky, *Principles of Induction Logging*. Amsterdam, The Netherlands: Elsevier, 2003, pp. 1–637.

[41] R. Streich, M. Becken, and O. Ritter, "2.5D controlled-source EM modeling with general 3D source geometries," *Geophysics*, vol. 76, no. 6, pp. F387–F393, 2012.

[42] J. Dang, Q. Zhao, C. Guo, J. Li, L. Zhang, and B. Dang, "Multi-coil array for long-distance cross-well electromagnetic detection," in *Proc. Int. Conf. Intell. Control, Meas., Signal Process. Intell. Oil Field.*, 2021, pp. 307–311.

[43] D. L. Alumbaugh and H. F. Morrison, "Monitoring subsurface changes over time with cross-well electromagnetic tomography," *Geophys. Prospecting*, vol. 43, no. 7, pp. 873–902, Jan. 1995.

[44] G. A. Newman and D. L. Alumbaugh, "Three-dimensional massively parallel electromagnetic inversion—I. Theory," *Geophys. J. Int.*, vol. 128, no. 2, pp. 345–354, Feb. 1997.

[45] D. L. Alumbaugh and G. A. Newman, "Three-dimensional massively parallel electromagnetic inversion—II. Analysis of a crosswell electromagnetic experiment," *Geophys. J. Int.*, vol. 128, no. 2, pp. 355–363, Feb. 1997.

[46] Q. H. Liu, "Reconstruction of two-dimensional axisymmetric inhomogeneous media," *IEEE Trans. Geosci. Remote Sens.*, vol. 31, no. 3, pp. 587–594, May 1993.

[47] K. Key, "MARE2DEM: A 2-D inversion code for controlled-source electromagnetic and magnetotelluric data," *Geophys. J. Int.*, vol. 207, no. 1, pp. 571–588, 2016.

[48] X. Wang, J. Shen, and B. Su, "3-D crosswell electromagnetic inversion based on general measures," *IEEE Trans. Geosci. Remote Sens.*, vol. 59, no. 11, pp. 9783–9795, Nov. 2021.

[49] P. Bai, G. Vignoli, and T. M. Hansen, "1D stochastic inversion of airborne time-domain electromagnetic data with realistic prior and accounting for the forward modeling error," *Remote Sens.*, vol. 13, no. 19, 2021, Art. no. 3881.

[50] G. Vignoli, J. Guillemoteauet, J. Barreto, and M. Rossi, "Reconstruction, with tunable sparsity levels, of shear-wave velocity profiles from surface wave data," *Geophys. J. Int.*, vol. 225, no. 3, pp. 1935–1951, Feb. 2021.

[51] G. Vignoli, V. Sapia, A. Menghini, and A. Viezzoliet, "Examples of improved inversion of different airborne electromagnetic datasets via sharp regularization," *J. Environ. Eng. Geophys.*, vol. 22, no. 1, pp. 51–61, 2017.

Jingxin Dang (Student Member, IEEE) received the B.S. degree in electrical engineering and automation from Xi'an Polytechnic University, Xi'an, China, in 2018, and the M.S. degree in electronic engineering with management from King's College London, London, U.K., in 2020. She is currently working toward the Ph.D. degree in information and communication engineering with the University of Electronic Science and Technology of China, Chengdu, China.

Her research interests include signal processing, electromagnetic logging, and electromagnetic imaging.

Qing Zhao received the B.S. degree in nuclear science from Chengdu University of Technology, Chengdu, China, in 1988, the M.S. degree in nuclear physics from Sichuan University, Sichuan, China, in 1998, and the Ph.D. degree in applied plasma physics from the Southwestern Institute of Physics, Chengdu, in 2001.

In 2001, he joined the High Power Microwave (HPM) Source Group, School of Physical Electronics, University of Electronic Science and Technology of China (UESTC), Chengdu, China, and in 2018, he joined the School of Resources and Environment, UESTC. His research interests include well logging, ground-penetrating radar, plasma effects on HPM sources, low-temperature plasma applications, the surface modification of materials, metamaterials, and artificial intelligence.

Cheng Guo received the Ph.D. degree in nuclear technology and applications from Chengdu University of Technology, Chengdu, China, in 2017.

He is currently a Postdoctoral Research Associate in information and communication engineering with the University of Electronic Science and Technology of China, Chengdu. His research interests include signal acquisition and processing, radiation detection and imaging.

Jiadai Li received the B.S. degree from the China University of Geosciences, Beijing, China, in 2015, and the Ph.D. degree in geology with the Institute of Geology and Geophysics, Chinese Academy of Sciences, Beijing.

After her Ph.D. studies, she was a Postdoctoral Fellow with the University of Electronic Science and Technology of China, Chengdu, China. Her research interests include electromagnetic detection, electromagnetic data interpretation, and artificial intelligence.

Lei Zhang is currently working toward the master's degree in electronic and information engineering with the School of Resources and Environment, University of Electronic Science and Technology of China (UESTC), Chengdu, China.

Tianzhi Tang was born in 1962. He is currently a Professorate Senior Engineer with China National Logging Corporation, Beijing, China. His research interests include logging method research, detection instrument development, and data processing and interpretation.

Bo Dang (Member, IEEE) was born in Xi'an China, in 1987. He received the Ph.D. degree in signal and information processing from Xidian University, Xi'an, China, in 2013.

Since 2014, he has been taught with the Department of Electronic Engineering, Xi'an Shiyou University, Xi'an, China. He is currently an Assistant Professor with the Department of Electronic Engineering. His research interests include downhole transient electromagnetic system for nondestructive testing and evaluation of casing and tubing.

Ling Yang (Student Member, IEEE) was born in Shaanxi, China, in 1993. She is currently working toward the Ph.D. degree in oil and gas engineering with Xi'an Shiyou University, Xi'an, China.

Her research interests include downhole transient electromagnetic oil and gas resource detection.

Changzan Liu (Student Member, IEEE) was born in Hebei, China, in 1989. He is currently working toward the Ph.D. degree in information and communication engineering with Northwestern Polytechnical University, Xi'an, China.

His research interests include downhole transient electromagnetic system for reservoir exploration.